Science and Technology Indonesia
e-ISSN:2580-4391 *p*-ISSN:2580-4405
Vol. 6, No. 4, October 2021

Research Paper

Biogenic Silica Extracted from *Salacca* Leaf Ash for Salicylic Acid Adsorption

Is Fatimah[1]*, Faiha Ulfiyani Zaenuri[1], Lolita Narulita Doewandono[1], Amri Yahya[1], Putwi Widya Citradewi[1], Suresh Sagadevan[2], Won-Chun Oh[3]

[1]*Chemistry Department, Universitas Islam Indonesia, Yogyakarta 55584, Indonesia*
[2]*Nanotechnology & Catalysis Research Center, University of Malaya, Kuala Lumpur 50603, Malaysia*
[3]*Department of Advanced Materials Science and Engineering, Hanseo University, Seosan-si, Chungnam 356–706, South Korea*
***Corresponding author**: isfatimah@uii.ac.id

Abstract
The extraction of biogenic silica from *Salacca* leaf ash and its utilization as an adsorbent for salicylic acid has been successfully conducted. The caustic extraction by refluxing the ash in NaOH followed by slow titration using acid produced the silica gel. The sintering of the dried gel was varied at 300, 400, and 500°C to evaluate its physicochemical character for adsorption purposes. Instrumental analysis of X-ray diffraction, scanning electron microscopy, gas sorption analysis, and Fourier transform infrared spectroscopy (FTIR) were employed. The kinetics of salicylic acid adsorption was investigated in a batch adsorption system and showed the fitness of the adsorption with a pseudo-second-order kinetics. The isotherm studies revealed that salicylic acid adsorption obeyed the Langmuir model. At varied sintering temperatures, the highest adsorption capacity and affinity were achieved at a temperature of 500°C, due to the increasing specific surface area. The maximum adsorption capacity of 36.7 mg/g is comparable with other work, but at less cost and synthesis process. The varied pH for adsorption is a suggestion that the neutral pH is the most feasible compared to the acidic and basic conditions.

Keywords
Adsorption, Biogenic Silica, Salicylic Acid

Received: 29 June 2021, Accepted: 18 September 2021
https://doi.org/10.26554/sti.2021.6.4.296-302

1. INTRODUCTION

The use of pharmaceuticals has significantly increased in recent decades and later due to the current COVID-19 pandemic. Many drugs and pharmaceutically active compounds (PACs) are produced in an extraordinarily significant amount. As a consequence, pharmaceutical waste from pharmacy industrial effluent is also increased. Besides, as a wastewater constituent, PACs are released during manufacturing and by disposal of unused or expired drugs. Due to their bioactivities, the removal and handling of many PACs must be appropriately designed to minimize environmental contamination. In the form of wastewater, standard technologies used for chemicals-containing water remediation are used for PACs treatment. Technologies based on advanced oxidation processes (AOP), adsorption, and electrochemical oxidation are popular treatment methods (Choi and Shin, 2020; Rakishev et al., 2021). The utilized low-cost materials, such as activated carbon, silica, and silica-alumina-based materials, have been explored to enhance the effectiveness of the PAC adsorption process.

High adsorptive capability, high efficacy, and good selectivity for removing a particular pharmaceutical compound are significant features for selecting substances to remove PACs from the environment. Salicylic acid (SA, $C_7H_6O_3$) is a critical compound in pharmaceutical industries that is widely used for some other pharmaceutical compounds, such as acetylsalicylic acid (ASA, $C_9H_8O_4$) and atenolol (ATL, $C_{14}H_{22}N_2O_3$). It is estimated that 40,000 tons of SA are consumed annually, and a high percentage of SA waste is released annually. The lack of specific SA treatment in wastewater management must cause adverse effects on the aquatic environment and biodiversity. Moderate to high toxic effects are caused by environmental SA exposure to aquatic organisms, including oxidative stress and toxicity (Freitas et al., 2020; Gómez-Oliván et al., 2014; Nunes, 2019). SA is a common and widely used analgesic, antipyretic, and anti-inflammatory drug, with an estimated annual consumption of 50–120 billion pills. Exploring adsorption preparation for SA adsorption will be critical in sustainable pharmaceutical industries (Choi and Shin, 2020).

In many studies, the use of some SA adsorbents, such as natural zeolite (clinoptilolite), clays (bentonite and kaolin), activated carbon, and other polymeric resins (Rakić et al., 2013; Otero et al., 2004), is reported. Silica and its building blocks,

such as MCM-41, have also been reported to have high SA adsorption efficacy. The SA adsorption using silica-based materials is not only proposed for water remediation, but it is also used as preconcentration and drug loading in slow-release drug preparation. As part of the exploration of new and renewable materials from the perspective of green chemistry, the use of biogenic silica for this purpose was proposed to improve economic benefits.

The high potency of *Salacca* leaf ash as a silica source was reported in previous works. The leaves are an agricultural waste produced in high amounts (Silviana and Bayu, 2018). The industrial utilization of *Salacca* leaves as a source of biogenic silica provides economic value for the industrial and agricultural sectors. Based on this background, this research was aimed to use biogenic silica extraction from the ash of *Salacca* leaves for SA adsorption. The potential content of silica in *Salacca* leaf ash (SLA) was revealed in previous investigations, but a more detailed study reporting its use as an SA adsorbent was not registered yet. Therefore, biogenic silica extraction for SA adsorption, considering the extraction method for creating specific physicochemical characteristics as an adsorbent, was performed in this study. As an adopted extraction method from the standard method of biogenic silica extraction from other sources, this study was focused on the effect of the silica sintering process on its physicochemical characteristics and SA adsorption capability.

2. EXPERIMENTAL SECTION

2.1 Materials

Salacca leaves were obtained from an agricultural area in the Sleman District, Yogyakarta, Indonesia. Chemicals used to extract silica from the *Salacca* leaves consisted of NaOH (97%), HCl (30%), SA (99%), and ammonium phosphate (99%). Such substances were purchased from Merck-Millipore (Germany) for pro analyst quality.

2.2 Method

The SLA was obtained by pre-treatment, which consisted of cleaning them with water and then drying them in an oven at 60°C. Later, the cleaned and dried leaves were incinerated in a muffle furnace at 500°C under atmospheric conditions for 2 h. Silica extraction was performed by refluxing 10 g of SLA with 100 ml of 1 M NaOH solution for 1 h. The result was filtered, and the filtrate was adjusted to pH 7.4 by dropping HCl 1 M until a white gel was produced. The precipitate was then kept in a hot air oven at 80°C overnight before sintering at varying temperatures: 300, 400, and 500°C. The samples were encoded as SiO_2-300, SiO_2-400, and SiO_2-500, respectively. The physicochemical characterization of the materials was performed using X-ray diffraction (XRD), a gas sorption analyzer, a Fourier transform infrared (FTIR) spectrophotometry, and scanning electron microscope-energy dispersive X-ray spectrophotometry (SEM-EDS). A Bruker D2 Phase 2^{nd} Gen X-ray diffractometer was employed in the analysis. A Ni-filtered Cu Kα ray (λ = 1.54056 Å) was used as a radiation source, and the measurements were carried out from 2θ = 10° to 80° at a rate of 0.4°/min. For the gas sorption analysis, a NOVA 1200 instrument was employed. For each analysis, the samples were degassed at 90°C for 4 h before analysis. /A Perkin-Elmer FTIR spectrophotometer was used in the analysis, and a Phenom X instrument was used in the SEM-EDS analysis. The schematic representation of the silica extraction method is shown in Figure 1.

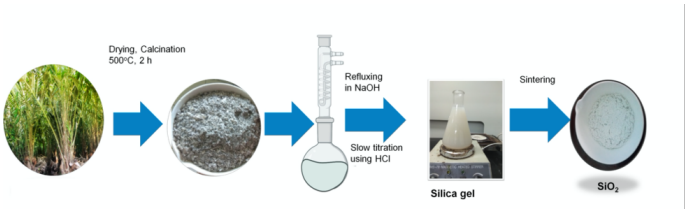

Figure 1. Schemtic Representation of The Method for Biogenic Silica Extraction

2.3 Adsorption Experiment

The SA adsorption experiments were conducted in a batch system using a bench horizontal shaker at 600 rpm. The SA analysis was performed on a UV-Visible spectrophotometric analysis based on a standard curve.

3. RESULTS AND DISCUSSION

3.1 Material Characterization

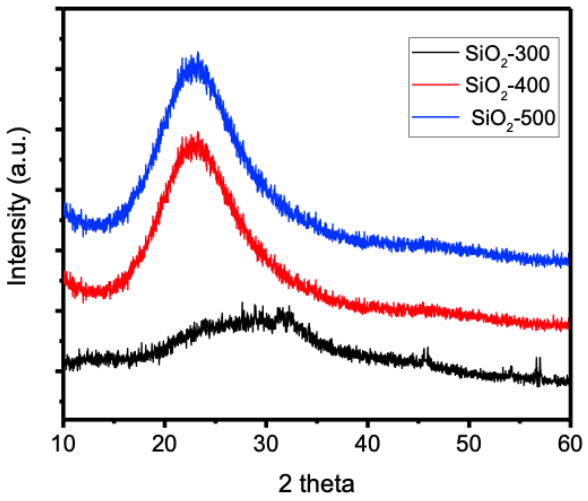

Figure 2. XRD Pattern of Derived SiO_2

The extracted silica at varying sintering temperatures was detected through XRD measurement with the reflections shown in Figure 2. A broad peak at a 2θ value of about 22° was exhibited by the XRD patterns in all samples. The broadness of these exhibited peaks are a confirmation that the synthesized biogenic nano silica samples were naturally amorphous

and were fitted with the JCPDS data file No: JCPDS 46-1045 (Chun et al., 2020; Fatimah et al., 2019; Jaafari et al., 2020).

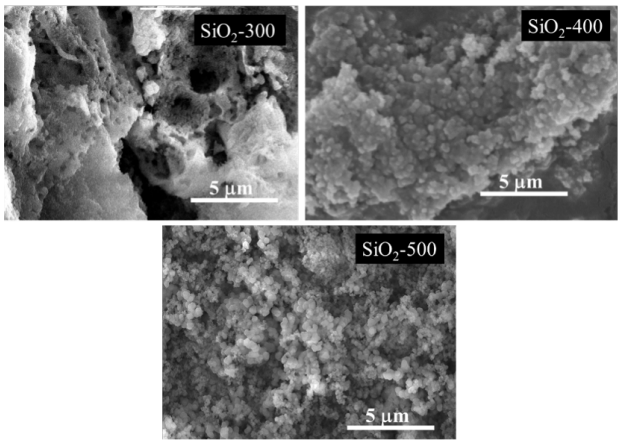

Figure 3. SEM Profile of Derived SiO_2 Samples

A higher peak intensity and the removal of some other peaks reflecting the impurities in the SiO_2-300 sample were caused by the sintering. However, the SiO_2 content was not influenced by the sintering temperature in the EDX analysis, suggesting that the impurities corresponded to silicious materials. The increasing intensity and the broad peak shift at the lower angle were attributed to the increasing pore size homogeneity caused by H_2O removal and dehydration at increasing temperatures. A similar effect was observed in silica extraction from rice husk ash and the characteristics of silica forms (Alyosef et al., 2013; Prasad and Pandey, 2012). The determined SiO_2 content was around 98.7–98.8% wt. The removal of the exhibited minor peaks and dehydration at the higher temperature was confirmed by the surface morphology change, as shown in Figure 3. More homogeneous particle sizes and a more opening surface were found for SiO_2-500. The surface morphology profiles of the samples are in agreement with the surface profile data obtained by gas sorption analysis.

Table 1. Surface Parameters and SiO_2 Content of Materials

Parameter	SiO_2-300	SiO_2-400	SiO_2-500
Specific surface area (m^2/g)	58.9	89.7	92.9
Pore radius (Å)	10.9	12.2	11.8
Pore volume (cc/g)	5.26×10^{-3}	23.1×10^{-3}	25.6×10^{-3}
SiO_2 content (% wt)	98.7	98.7	98.8

The sintering temperature effect on the surface was also identified from the change of specific surface area, and pore distribution, shown in Figure 4. The calculated parameters are shown in Table 1. The specific surface area of 58.9 m^2/g was demonstrated by the prepared SiO_2. After the sintering process, it was increased to 89.7 m^2/g and 92.9 m^2/g at 300°C and 500°C, respectively. The increased specific surface area is consistent with the adsorption-desorption profile Figure 4 and the pore size distribution Figure 4, reflecting the improvement in adsorption capability at all the P/P° ranges. The microporous domination, which is characteristic of silica and nano silica extracted from biogenic sources, was implied by the isotherm pattern and pore distribution plots.

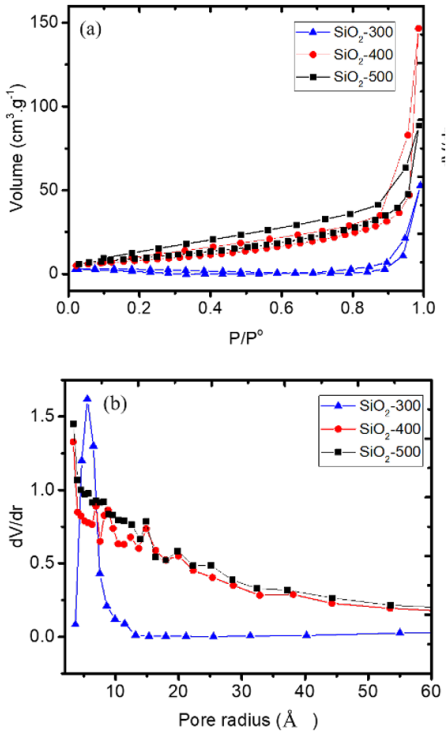

Figure 4. Adsorption-Desorption Isotherm of SiO_2 samples (a), Pore Distribution Curve of SiO_2 Samples (b)

The comparison of silica content and the specific surface area from various silica sources are shown in Table 2. In other sources in which a high specific surface area (more than 100 m^2/g) was exhibited, such as oat and rice husks, the specific surface area of SiO_2 obtained in this research was relatively lower (more than 99% wt) with high specific surface area (more than 100 m^2/g), but the silica content is relatively high (98.7% wt).

The FTIR spectra comparison is shown in Figure 5 shows. There was no significant difference among the materials. The -OH absorptions were identified at a wavenumber of around 3388.9–3394.1 cm^{-1}, and the lower wavenumber (3388.9 cm^{-1}) corresponded to SiO_2-300. The band was unidentified at a higher calcination temperature, indicating the reduced amount of -OH functional group on the surface caused by the heating and dehydration process. The absorption bands at 1633–1638 cm^{-1} were representations of the asymmetric stretching vibrations Si-O-Si stretching vibration, following the Si-O symmetric stretching vibration identified at a wavenumber of around 1387 cm^{-1}. Other absorption bands around 430–460 cm^{-1} are indications of Si-O bending vibrations.

Table 2. Comparison of SiO_2 Specific Surface Area and Content Obtained from Various Sources

Source	Silica content (%wt)	Specific surface area (m^2/g)	Reference
Rice husk	97.7	313	(Alyosef et al., 2013)
Sugarcane baggase	87.6	15	(Alyosef et al., 2013)
Oat husk	99.1	248	(Maseko et al., 2021)
	91.6	301	(Maseko et al., 2021)
Ground nut shell	nd	0.89	(Peerzada and Chidambaram, 2020)
Oat husk	94.1–94.3	124–129	(Mattos et al., 2016)
Horsetail	98.2	393	(Mattos et al., 2016)
Bamboo leaves ash	99.1	428	(Rangaraj and Venkatachalam, 2017)
Salacca leaves ash	98.7	58.9	This work

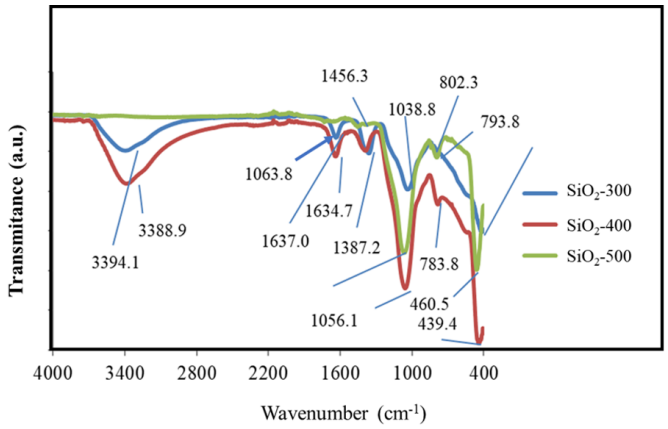

Figure 5. FTIR Spectra of Materials

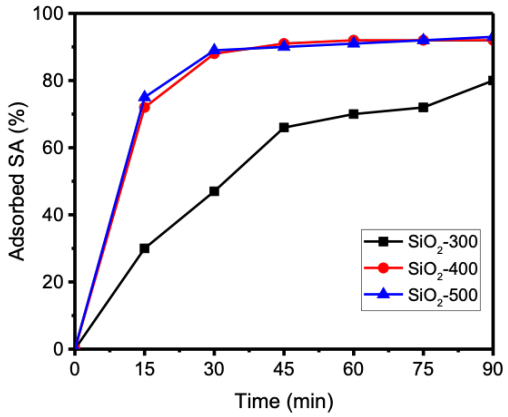

Figure 6. Kinetics of SA Adsorption on SiO_2 Samples [Initial SA Concentration = 20 mg/L, Temperature = 25°C, pH = 7]

3.2 Adsorption of SA

The SA adsorption kinetics were evaluated by referring to the pseudo-first-order and pseudo-second-order by the following equations 1– 2 :

$$ln(q_e - q_t) = lnq_e - kt \quad (1)$$

$$\frac{t}{q_t} = \frac{1}{k_2 q_e^2} + \frac{t}{q_e} \quad (2)$$

where, q_t (mg/g) is the amount of adsorbed metal ions at the time of t, q_e (mg/g) is adsorption capacity, k (min^{-1}) is the first-order rate constant, and k_2 (g/mg min) is the second-order rate constant of adsorption (min^{-1}) (Lee et al., 2018; Zou et al., 2018).

SA adsorption kinetics are shown by the curve in Figure 6. Insignificant adsorption capabilities were exhibited by the SiO_2-400 and SiO_2-500 with the varied sintering temperature. Nonetheless, such numbers were still higher than those for SiO_2-300.

The higher R^2 values for the pseudo-second-order kinetics model for all adsorbents are suggestions for the second-order fitness. The kinetics order represented the dependency of the adsorption mechanism concerning both the SA concentration and the available adsorption sites. SA adsorption was also obtained using polymeric and activated carbon in a similar kinetics study (Câmara and Neto, 2008). Given the chemical SA structure, which contains the hydroxyl functional groups and the aromatic ring, hydrogen bonding and electrostatic interaction are the main mechanisms besides the possible molecular sieving mechanism. Given the silica surface interaction with some other aromatic compounds, the net negative charge of the aromatic ring is electrostatically bound with the oxygen on the silica surface. Meanwhile, the hydrogen atom interacts with the surface via hydrogen bonding (Sadhu et al., 2014; Yuan et al., 2019). The schematic representation of the adsorption mechanism is shown in Figure 6.

The adsorption isotherm was performed by modeling the adsorption data using the Langmuir and Freundlich models to study the interaction between the adsorbate and adsorbent. The Freundlich and Langmuir model equations are represented in the following equations 3–4:

Table 3. The Calculated Langmuir and Fruendlich Isotherm Parameters

Adsorbent	Langmuir				Freundlich		
	q_m (mg/g)	K_L (L/mg)	R_L	R^2	K_F (L/g)	1/n	R^2
SiO_2-300	26.58	2.11	0.93	0.997	1.32	0.28	0.931
SiO_2-400	26.51	1.86	0.93	0.997	1.33	0.29	0.916
SiO_2-500	34.91	8.21	0.8	0.981	1.49	0.39	0.945

$$q_e = K_F C_e^{1/n} \tag{3}$$

$$q_e = \frac{q_m K_L C_e}{1 + K_L C_e} \tag{4}$$

where q_e (mg/g) is the equilibrium adsorption capacity of the adsorbent, C_e (mg/L) is the concentration of adsorbate in equilibrium, q_m (mg/g) is the maximum adsorptive capacity of the adsorbent, K_F is the Freundlich constant related to the adsorption-desorption equilibrium of adsorption capacity, n is the Freundlich constant related to the adsorption intensity, and K_L (L/mg) is the Langmuir constant related to the adsorption energy (Dada et al., 2012).

The equilibrium parameter from the Langmuir isotherm, RL, is represented as follows equation 5 :

$$RL = \frac{1}{1 + K_L q_m} \tag{5}$$

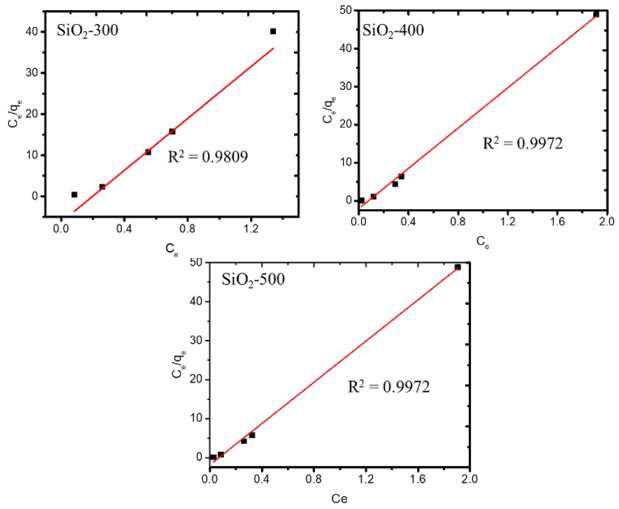

Figure 7. Linear Langmuir Model Plot of SA Adsorption by SiO_2 Samples

The calculated parameters are shown in Table 3. From the values, it was observed that both models applied well for SA adsorption in all SiO_2 samples. However, the Langmuir model was better based on the nearness to the unity of the R^2 values. This finding is also shown in Figure 7, where the fitness of adsorption data with the Langmuir model was implied. A typical surface diffusion control of the adsorption by a homogeneous surface was demonstrated by the fitness of the Langmuir model (Câmara and Neto, 2008). The role of chemisorption on the silica surface was validated by the 1/n values from the Freundlich isotherm that was laid at 1/n < 1, and by the Langmuir model, the RL values ranged from 0 < R_L < 1 (0.80–0.94) for all adsorbents. In previous similar works, it was stated that the RL values = 0, 0 < R_L < 1, R_L = 1, and R_L > 1 are indicative of irreversible, favorable, linear, and unfavorable adsorption, respectively. The SA adsorption from all the samples in this work was favorable (Yagub et al., 2014).

Table 4. Comparison of SA Adsorption Capacity Using Various Adsorbents

Adsorbent	Adsorption Capacity (mg/g)	Reference
Zeolite	8.97	(Rakić et al., 2013)
Zeolite	2.3	(Cabrera-Lafaurie et al., 2014)
Bentonite	34.5	(Rakishev et al., 2021)
Activated Carbon	4.2	(Rakishev et al., 2021)
Non-Imprinted Polymer (NIP)	63.5	(Xu et al., 2021)
Hexadecyltrimethy lammonium-Modified Montmorillonite	42	(Choi and Shin, 2020)
Molecularly Imprinted Chitosan	30.42	(Rahangdale et al., 2016)
Graphene	63.66	(Lee et al., 2018)
Molecularly Imprinted Polymer	30.3	(Rahangdale et al., 2016)
Si-500	36.7	This work

From the varied sintering temperature, the SiO_2-500 was suggested by all parameters from both isotherms to have the highest affinity for SA adsorption. The adsorption affinity was in line with the specific surface area data, indicating that a higher sintering temperature produced a higher specific surface area. Based on the adsorption capability data and the comparison with other adsorbents presented in Table 4, the SA adsorption

by the biogenic silica extracted in this research was comparable to that obtained from bentonite and was even higher than that obtained from zeolite. With a capacity of 36.7 mg/g, the SiO_2-500 sample give higher value compared to molecularly imprinted polymer and molecularly imprinted chitosan, even though it is still lower compared to other adsorbents. It is important to be noted that the synthesis method in this work is by the lower cost.

3.3 Effect of pH

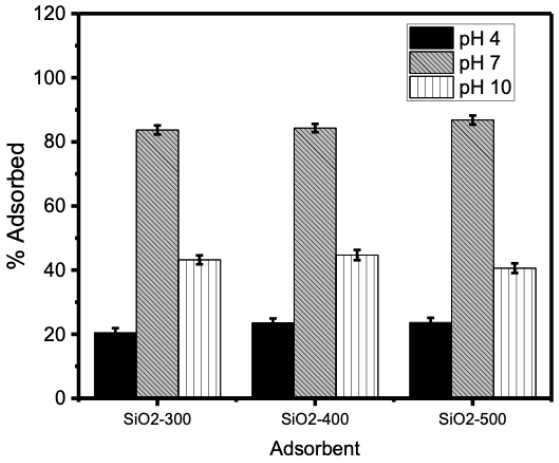

Figure 8. Effect of pH on SA Adsorption Capacity by The Materials

The study of the effect of pH on adsorption capability is of critical importance for the application purpose. The varying pH of 4, 7, and 9 on the SA adsorbed percentage is shown in Figure 8. There was optimum adsorption at the neutral (pH = 7) from these values, which was identified by the highest SA adsorption percentage for all SiO_2 samples. The lower adsorption capacity at a low pH (pH = 4) is attributed to the protonic condition of the silica surface. Therefore, there was a repulsive force on the SA surface. Contrarily, the negative charge of the surface was led by the basic condition (pH = 10), according to equation 6, as follows:

$$SiOH + OH^- > SiO^- + H_2O \quad (6)$$

Repulsive force may occur due to the hydroxyl group in SA (Mustafa et al., 2003). The adsorption mechanism is suggested to be intensely dependent on the surface charge by the results. This finding is characteristic of adsorption, with no other mechanism, such as covalent, ligan-metal ion, or π-π interaction.

4. CONCLUSIONS

In this study, biogenic silica was successfully extracted from *Salacca* leaf ash, and the silica samples were shown to be effective adsorbents for salicylic acid from an aqueous solution. The increasing specific surface area and the increasing temperature were reflected by the varying sintering temperatures, which affected the increasing adsorption capacity. The homogeneous surface of silica was exhibited, as suggested by the fitness of the adsorption kinetics to the Langmuir isotherm model. The results of this research represented that *Salacca* leaf ash is potential resource for biogenic silica production. The exploration on other modifications for enhancing the capability of the material in industrial scale should be conducted intensively.

5. ACKNOWLEDGEMENT

Authors thank to Chemistry Department, Universitas Islam Indonesia for supporting this research in Research Excellencies Facilities and International Collaboration Program.

REFERENCES

Alyosef, H. A., A. Eilert, J. Welscher, S. S. Ibrahim, R. Denecke, W. Schwieger, and D. Enke (2013). Characterization of biogenic silica generated by thermo chemical treatment of rice husk. *Particulate Science and Technology*, **31**(5); 524–532

Cabrera-Lafaurie, W. A., F. R. Román, and A. J. Hernández-Maldonado (2014). Removal of salicylic acid and carbamazepine from aqueous solution with Y-zeolites modified with extraframework transition metal and surfactant cations: equilibrium and fixed-bed adsorption. *Journal of Environmental Chemical Engineering*, **2**(2); 899–906

Câmara, L. and A. S. Neto (2008). MODELING OF THE KINETIC OF SALICYLIC ACID ADSORPTION IN POLYMERIC AND ACTIVATED CHARCOAL ADSORBENTS. *Revista de Engenharia Térmica*, **7**(1); 49–54

Choi, J. and W. S. Shin (2020). Removal of Salicylic and Ibuprofen by Hexadecyltrimethylammonium-Modified Montmorillonite and Zeolite. *Minerals*, **10**(10); 898

Chun, J., Y. M. Gu, J. Hwang, K. K. Oh, and J. H. Lee (2020). Synthesis of ordered mesoporous silica with various pore structures using high-purity silica extracted from rice husk. *Journal of industrial and engineering chemistry*, **81**; 135–143

Dada, A., A. Olalekan, A. Olatunya, and O. Dada (2012). Langmuir, Freundlich, Temkin and Dubinin–Radushkevich isotherms studies of equilibrium sorption of Zn2+ unto phosphoric acid modified rice husk. *IOSR Journal of Applied Chemistry*, **3**(1); 38–45

Fatimah, I., S. N. Amaliah, M. F. Andrian, T. P. Handayani, R. Nurillahi, N. I. Prakoso, W. P. Wicaksono, and L. Chuenchom (2019). Iron oxide nanoparticles supported on biogenic silica derived from bamboo leaf ash for rhodamine B photodegradation. *Sustainable Chemistry and Pharmacy*, **13**(3); 100149

Freitas, R., S. Silvestro, F. Coppola, V. Meucci, F. Battaglia, L. Intorre, A. M. Soares, C. Pretti, and C. Faggio (2020). Combined effects of salinity changes and salicylic acid exposure in Mytilus galloprovincialis. *Science of the Total Environment*, **715**; 136804

Gómez-Oliván, L. M., M. Galar-Martínez, H. Islas-Flores,

S. García-Medina, and N. SanJuan-Reyes (2014). DNA damage and oxidative stress induced by acetylsalicylic acid in Daphnia magna. *Comparative Biochemistry and Physiology Part C: Toxicology & Pharmacology*, **164**; 21–26

Jaafari, S. A. A. H., J. Athinarayanan, V. S. Periasamy, and A. A. Alshatwi (2020). Biogenic silica nanostructures derived from Sorghum bicolor induced osteogenic differentiation through BSP, BMP-2 and BMP-4 gene expression. *Process Biochemistry*, **91**(12); 231–240

Lee, W., S. Yoon, J. K. Choe, M. Lee, and Y. Choi (2018). Anionic surfactant modification of activated carbon for enhancing adsorption of ammonium ion from aqueous solution. *Science of the Total Environment*, **639**; 1432–1439

Maseko, N. N., D. Schneider, S. Wassersleben, D. Enke, S. A. Iwarere, J. Pocock, and A. Stark (2021). The Production of Biogenic Silica from Different South African Agricultural Residues through a Thermo-Chemical Treatment Method. *Sustainability*, **13**(2); 577

Mattos, B. D., O. J. Rojas, and W. L. Magalhães (2016). Biogenic SiO2 in colloidal dispersions via ball milling and ultrasonication. *Powder Technology*, **301**; 58–64

Mustafa, S., B. Dilara, A. Naeem, N. Rehana, and K. Nargis (2003). Temperature and pH effect on the sorption of divalent metal ions by silica gel. *Adsorption Science & Technology*, **21**(4); 297–307

Nunes, B. (2019). Acute ecotoxicological effects of salicylic acid on the Polychaeta species Hediste diversicolor: evidences of low to moderate pro-oxidative effects. *Environmental Science and Pollution Research*, **26**(8); 7873–7882

Otero, M., C. A. Grande, and A. E. Rodrigues (2004). Adsorption of Salicylic Acid onto Polymeric Adsorbents and Activated Charcoal. *Reactive and Functional Polymers*, **60**; 203–213

Peerzada, J. G. and R. Chidambaram (2020). A Statistical Approach for Biogenic Synthesis of Nano-Silica from Different Agro-Wastes. *Silicon*, **13**(7); 1–13

Prasad, R. and M. Pandey (2012). Rice husk ash as a renewable source for the production of value added silica gel and its application: an overview. *Bulletin of Chemical Reaction Engineering and Catalysis*, **7**(1); 1–25

Rahangdale, D., G. Archana, and A. Kumar (2016). Molecularly imprinted chitosan-based adsorbents for the removal of salicylic acid and its molecular modeling to study the influence of intramolecular hydrogen bonding of template on molecular recognition of molecularly imprinted polymer. *Adsorption Science & Technology*, **34**(7-8); 405–425

Rakić, V., N. Rajić, A. Daković, and A. Auroux (2013). The adsorption of salicylic acid, acetylsalicylic acid and atenolol from aqueous solutions onto natural zeolites and clays: Clinoptilolite, bentonite and kaolin. *Microporous and Mesoporous Materials*, **166**; 185–194

Rakishev, A., M. Vedenyapina, S. Kulaishin, and D. Kurilov (2021). Adsorption of Salicylic Acid from Aqueous Solutions on Microporous Granular Activated Carbon. *Solid Fuel Chemistry*, **55**(2); 117–122

Rangaraj, S. and R. Venkatachalam (2017). A lucrative chemical processing of bamboo leaf biomass to synthesize biocompatible amorphous silica nanoparticles of biomedical importance. *Applied Nanoscience*, **7**(5); 145–153

Sadhu, K., A. Mukherjee, S. K. Shukla, K. Adhikari, and S. Dutta (2014). Adsorptive removal of phenol from coke-oven wastewater using Gondwana shale, India: experiment, modeling and optimization. *Desalination and Water Treatment*, **52**(34-36); 6492–6504

Silviana, S. and W. J. Bayu (2018). Silicon conversion from bamboo leaf silica by magnesiothermic reduction for development of Li-ion baterry anode. In *Matec web of conferences*, volume 156. EDP Sciences, page 05021

Xu, H., Y. Gao, Q. Tao, A. Li, Z. Liu, Y. Jiang, H. Liu, R. Yang, and Y. Liu (2021). Synthesizing a surface-imprinted polymer based on the nanoreactor SBA-15 for optimizing the adsorption of salicylic acid from aqueous solution by response surface methodology. *New Journal of Chemistry*, **45**(14); 6192–6205

Yagub, M., T. Sen, S. Afroze, and H. Ang (2014). Dye and its removal from aqueous solution by adsorption: a review. Adv Colloid Interfac 209: 172–184

Yuan, N., H. Cai, T. Liu, Q. Huang, and X. Zhang (2019). Adsorptive removal of methylene blue from aqueous solution using coal fly ash-derived mesoporous silica material. *Adsorption Science & Technology*, **37**(3-4); 333–348

Zou, C., J. Liang, W. Jiang, Y. Guan, and Y. Zhang (2018). Adsorption behavior of magnetic bentonite for removing Hg (II) from aqueous solutions. *RSC advances*, **8**(48); 27587–27595

